Identification of Early Proteomic Markers for Hepatic Steatosis

ARTICLE *in* CHEMICAL RESEARCH IN TOXICOLOGY · SEPTEMBER 2006

Impact Factor: 3.53 · DOI: 10.1021/tx060007f · Source: PubMed

7 AUTHORS, INCLUDING:

Paul C Guest
University of Cambridge
167 PUBLICATIONS **2,711** CITATIONS

Chemical Profiles

Identification of Early Proteomic Markers for Hepatic Steatosis

G. Meneses-Lorente,*,‡ A. Watt,‡ K. Salim,‡ S. J. Gaskell,§ Nagaraja Muniappa,† Jeffrey Lawrence,† and P. C. Guest‡

Merck Sharp & Dohme Neuroscience Research Centre, Terlings Park, Harlow, Essex, CM20 2QR, United Kingdom, Michael Barber Centre for Mass Spectrometry, University of Manchester, Manchester M1 7ND, United Kingdom, and Department of Safety Assessment, Merck Research Laboratories, West Point, Pennsylvania 19486

Received January 13, 2006

The identification of biomarkers for disease state, drug efficacy, and toxicity is becoming increasingly important for drug discovery and development. We have used two-dimensional differential in-gel electrophoresis and mass spectrometry to identify proteomic markers associated with hepatocellular steatosis in rats after dosing with a compound (CDA) in preclinical development. Rats were dosed daily for up to 5 days with CDA for measurement of blood biochemical parameters, histological, and proteomic analysis. Alterations in plasma glucose and liver transaminases were detected from dosing day 3 onward, and livers showed trace levels of hepatocellular vacuolation from 6 h which increased in extent and severity over the 5 day time course. The number of significantly altered protein spots increased over the 5 day time course, and Ingenuity Pathway Analysis showed that the predominant functions altered by CDA treatment were cell death and cellular assembly and organization. This included alterations in secreted proteins, endoplasmic reticulum and mitochondrial chaperones, antioxidant proteins, and enzymes involved in fatty acid biosynthesis. Comparative in vitro dosing studies showed similar alterations to the proteome, neutral lipid accumulation, and mitochondrial dehydrogenase activity in response to CDA treatment of cultured rat hepatocytes. The finding that several proteins showed significant changes in abundance before the onset of overt toxicity in vivo suggested that these could serve as predictive biomarkers of compounds with a propensity to induce liver steatosis. These markers underwent further direct analysis in the in vitro hepatocyte toxicity model to determine their utility in the development of high throughput assays for drug-induced steatosis.

Introduction

A significant problem faced by pharmaceutical companies today is the failure of lead compounds in the later stages of development due to unexpected toxicities. Approximately 30% of new compounds fail due to toxicity, which results in increased costs and delays in drug development (*1*). Such toxicities are not likely to become apparent until the preclinical or clinical development stages when compound testing is initiated in animal models or humans. Therefore, the application and development of technologies that can predict toxicities within an in vivo/in vitro setting would facilitate the drug development process. Molecular profiling technologies such as proteomics are currently under intensive investigation by pharmaceutical companies to facilitate the development of assays which employ protein biomarkers or other reporters to predict drug-related toxicities (*2*).

In-house in vivo safety studies identified a compound (designated CDA) that was hepatotoxic in mice, rats, and monkeys causing steatosis, centrilobular granular hypertrophy, single-cell necrosis, and periductal inflammation (data not shown). We recently reported that the mechanism of this toxicity involved disruption of the β-oxidation pathway as identified through metabonomic (*3*) and proteomic (*4*) analyses. Previous reports have shown 4,4′-diethylaminoethoxyhexestrol, amiodarone, and perhexiline, which are known to cause steatohepatitis in humans, also inhibit β-oxidation and respiration in rat hepatocytes (*5*). Drug-induced steatosis is a serious issue for the pharmaceutical industry, since it could lead to liver failure resulting in withdrawing the compound from the market (*6*). The identification of novel early biomarkers from drug-induced steatosis could aid drug discovery by improving the toxicity decision process.

In our previous proteomics study, we used fluorescence two-dimensional (2D) differential in-gel electrophoresis (DIGE) (*7*, *8*) to investigate the mechanism of CDA-induced toxicity in rats after 6 h of treatment (*4*). We showed that the proteomics data correlated with the clinical and histological data and some of the proteomic changes occurred before the onset of overt toxicity. We have extended these studies by analyzing a latter stage of CDA-induced toxicity and by attempting to identify markers associated with the toxicity that could be converted into novel diagnostic marker assays. For the preliminary stages of this work, we established a correlation between the in vivo and in vitro proteomics studies using CDA-treated primary rat

* To whom correspondence should be addressed. Current address: Roche Products Limited, 6 Falcon Way, Shire Park, Welwyn Garden City, AL7 1TW, London, U.K. Phone: +44 (0) 1707 366467. E-mail: georgina.meneses-lorente@roche.com.

‡ Merck Sharp & Dohme Neuroscience Research Centre.

§ Michael Barber Centre for Mass Spectrometry, University of Manchester.

† Merck Research Laboratories.

10.1021/tx060007f CCC: $33.50
Published on Web 07/18/2006

Table 1. Experimental Design for 2D-DIGE Study on the Liver Proteomic Effects of CDA[a]

gel number	Cy2	Cy3	Cy5
1	pooled std	CDA-2	Veh-2
2	pooled std	CDA-2	Veh-2
3	Veh-2	pooled std	CDA-2
4	Veh-2	Pooled std	CDA-2
5	CDA-2	Veh-2	pooled std
6	CDA-2	Veh-2	pooled std
7	pooled std	CDA-5	Veh-5
8	pooled std	CDA-5	Veh-5
9	Veh-5	pooled std	CDA-5
10	Veh-5	pooled std	CDA-5
11	CDA-5	Veh-5	pooled std
12	CDA-5	Veh-5	Pooled Std

[a] Approximately 50 μg of soluble or insoluble liver extracts from rats treated with CDA or vehicle for 2 and 5 days and the pooled standard (equal mixture of all samples used in the experiment) was labeled with 0.2 nM of the indicated CyDye, mixed together as shown on 2D gels. Twelve gels were run as indicated for the separate soluble and insoluble protein extracts (24 gels total).

hepatocytes. This study also presents the application of a fluorescence-based, compound-screening assay for neutral lipid accumulation using rat hepatocytes based on the findings from the proteomics studies.

Experimental Procedures

Materials. The CyDyes (Cy2, Cy3, and Cy5) and Immobilized DryStrips (IPG strips) were purchased from Amersham Biosciences (Little Chalfont, Bucks., U.K.). Sypro Ruby fluorescent protein stain was obtained from Molecular Probes, Inc. (Eugene, OR). Sequencing-grade modified trypsin was from Promega (Madison, WI). All other biochemicals were obtained from Sigma (Poole, Dorsett, U.K.) unless specified otherwise.

Animals. Female Sprague−Dawley international standard rats (170−180 g) were supplied by Charles River (U.K.) and provided food (Bantin and Kingman rat and mouse expanded diet) and water ad libitum. All animal experiments were in accordance with the U.K. Home Office practices and procedures. Rats were dosed with 250 (mg/kg)/day CDA for 6 h, 2 days, and 5 days as described previously (*4*).

Hepatocyte Preparation and Culture. Rats were injected with 500 U of heparin 5 min prior to euthanasia. Livers were removed and placed into ice-cold Dulbecco's phosphate-buffered saline (DPBS), and the largest lobes were subjected to a two-stage perfusion procedure based on cut surface perfusion models (*9*). Following digestion with collagenase (Collagenase H, Boehringer Mannheim, Germany), cells were filtered through nylon bolting cloth and subjected to three rounds of centrifugation at 500*g* for 5 min at 4 °C and resuspension in sterile DPBS. Hepatocytes were finally resuspended at 1.5×10^5 viable cells/mL (as determined by trypan blue exclusion) in Williams' E Medium containing 2 mM L-glutamine, 100U/mL penicillin, 0.1 mg/mL streptomycin, 50 mg/mL gentamycin, 100 nM DEX, and 1μM insulin. Typical yields were 1.5×10^8 viable cells (>80% viability) per rat. Hepatocytes were dispensed into black clear-bottom and clear 96 well collagen-coated plates at 3×10^4 cells per well for fatty acid accumulation and mitochondrial dehydrogenase assays (below). For the proteomic studies, 1.8×10^6 cells were dispensed onto 6 cm collagen-coated dishes. After allowing cells to settle for 24 h at 37 °C in a CO_2 incubator with 95% humidity, nonviable cells and debris were aspirated and the media replaced. Following a further 24 h incubation, the cells were ready for treatment (below).

Cell Treatments. Stock solutions of CDA and amiodarone were prepared in sterile DMSO at a concentration of 10 mM. Compounds (n = 6 wells/treatment) were added directly to cells so that the

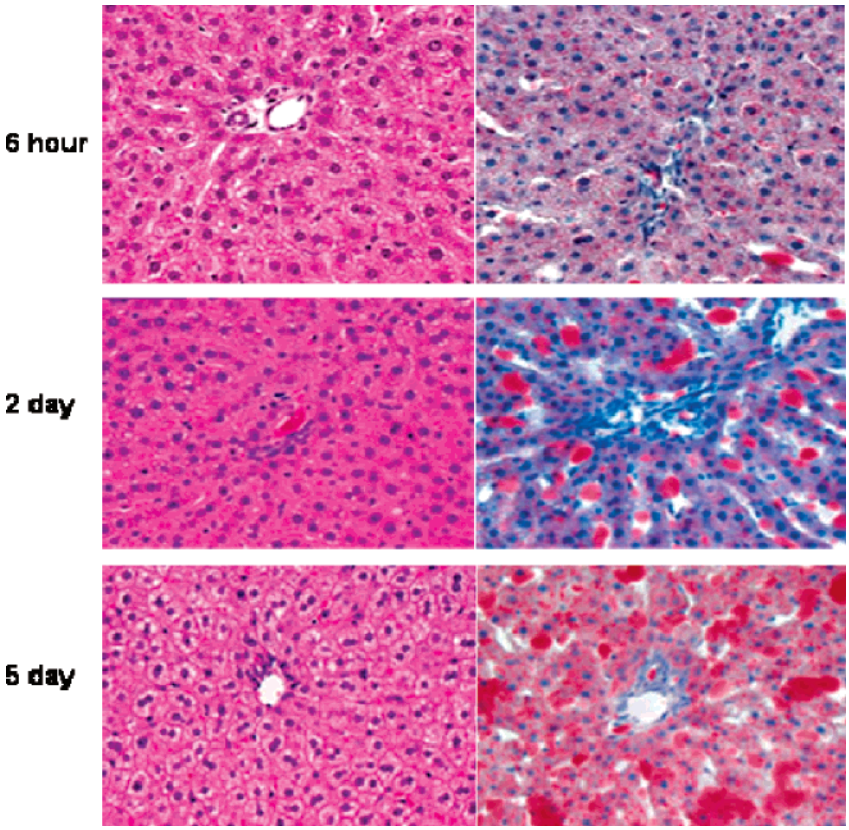

Figure 1. Light microscopic examination of rat liver sections following treatment with CDA. Rats were treated with 250 (mg/kg)/day CDA for the indicated times, and 50 μm liver sections were processed for histological examination as described previously (*4*). Images on the left are hematoxylin/eosin staining showing the presence of vacuoles in the cytoplasm of hepatocytes. Images on the right are Oil Red O staining showing lipid-filled (red staining) vesicles present in the cytoplasm of hepatocytes. Equivalent images were obtained with each of the three livers examined (incidence 3/3 animals).

Table 2. Identification of Soluble Liver Proteins Which Showed Altered Expression after Treatment with CDA[a]

spot	FC 2 day	FC 5 day	ANOVA	ACC	gene name	protein
351	−1.06	−1.39	3.0×10^{-5}	P46462	VCP	transitional endoplasmic reticulum ATPase
364	−1.12	−2.14	2.7×10^{-3}	P39052	DNM1	Dynamin 1
418	−1.30	−1.86	7.9×10^{-7}	ND	ND	ND
432	−1.23	−1.74	1.7×10^{-8}	ND	ND	ND
490	−1.21	−1.17	1.4×10^{-5}	P14882	PCCA	propionyl-CoA carboxylase
664	1.25	1.27	5.2×10^{-7}	ND	ND	ND
740	−1.98	−2.48	7.8×10^{-6}	Q10758	KRT8	cytokeratin 8
789	1.04	−1.73	1.8×10^{-2}	P11884	ALDH2	aldehyde dehydrogenase
820	−1.10	−1.30	2.2×10^{-5}	P04764	ENO1	α-enolase
832	−1.13	−2.65	1.0×10^{-5}	P05784	KRT18	cytokeratin 18
951	−1.14	−1.25	2.3×10^{-6}	Q64640	ADK	adenosine kinase
956	1.25	1.31	2.6×10^{-5}	Q96HG5	ACTB	*β* actin
1090	1.38	1.27	1.7×10^{-6}	O35077	GPD1	glycerol dehydrogenase
1123	−3.39	−2.86	3.6×10^{-6}	ND	ND	ND
1169	−1.25	−1.30	5.3×10^{-5}	128428443	-	RIKEN cDNA 2010317E03 gene
1180	−1.08	−1.25	1.1×10^{-3}	Q02974	KHK	ketohexokinase
1205	−1.25	−1.39	1.4×10^{-4}	P46953	HAAO	3-hydroxyanthranilate 3,4 dioxygenase
1309	−1.24	−1.25	3.7×10^{-4}	ND	ND	ND
1338	1.22	1.33	5.6×10^{-4}	ND	ND	ND
1350	−1.16	−1.66	2.4×10^{-2}	P22734	COMT	catechol *O*-methyltransferase
1362	−1.23	−1.32	4.8×10^{-4}	ND	ND	ND

[a] Protein spots indicated in Figure 2 were identified by MALDI-TOF mass fingerprinting and or Q-TOF MS/MS sequencing as described in Experimental Procedures. For each protein spot, the fold change (FC), ANOVA, protein accession number (ACC), gene names, and protein names are indicated. Only protein spots that were present on every gel and demonstrating changes of ± 0.10 with significance $p < 0.05$ were accepted as being differentially expressed. The levels of significance are given for three separate animal comparisons (each comparison carried out in duplicate incorporating reciprocal labeling). Nonidentified proteins are indicated by ND.

DMSO concentration was constant at 0.1% (v/v). DMSO was added as the negative control. CDA was tested over a concentration range from 75 to 600 μM. Amiodarone (positive control) was tested over a concentration range from 12.5 to 100 μM. After 24 h, the fatty acid accumulation and mitochondrial function assays were performed in black clear-bottom and clear 96-well culture plates, respectively.

Fatty Acid Accumulation Assay. The Nile Red fluorescent dye has been used previously to study fat accumulation in many types of cells (*10*). The assay was performed using the protocol previously described (*11*). After 24 h of treatment, cells were washed with Hank's buffered salt solution (HBSS), and the background fluorescence was determined using 535 nm excitation and 580 nm emission wavelengths in a Gemini plate reader (Molecular Devices). Nile Red was diluted from a 1 mM stock solution in DMSO containing 1% pluronic acid to a final concentration of 1 μM in HBSS, and 100 μL was added to each well. After 4 h incubation at room temperature in the dark, the supernatant containing Nile Red was removed and cells were washed once with HBSS. Cells were incubated for a further 16 h in HBSS at room temperature in the dark, and the fluorescence was measured in the Gemini plate reader using 535 nm excitation and 580 nm emission settings to selectively measure neutral lipids instead of the phospholipids, which can also be measured with Nile Red at different excitation and emission settings. Confocal imaging was performed using an Attofluor Ratiovision imager with a confocal Atto-Ratio Vision (CARV) module (Atto Instrument, Inc., Rockville, MD).

Mitochondrial Dehydrogenase Assay. The colorimetric in vitro toxicology assay utilized MTT (3-[4,5-dimethylthiazol-2-yl]-2,5-diphenyl tetrazolium bromide) as an indicator of mitochondrial dehydrogenase activity (*12*). After treatment of hepatocytes with CDA or amiodarone for 24 h, the media were removed and 40 μL of MTT was added to each well for a further 4 h incubation. Cells were removed from the incubator, and the MTT formazan crystals were dissolved by addition of 100 μL of 2-propanol. The absorbance was measured at a wavelength of 570 nm. Background plate absorbance was measured at 690 nm and subtracted from the 570 nm measurement.

Preparation of Protein Extracts for Proteomic Studies. Cell pellets and tissues were subjected to a differential solubility extraction procedure essentially as described (*13*). Homogenization was carried out at 4 °C using an MSE Soniprep 150 sonicator at an amplitude of 15 μm for 30 s in 30 mM Tris (pH8) buffer containing 8 M urea and complete EDTA-free protease inhibitors at 100 mg/mL tissue/buffer ratio. The homogenates were centrifuged at 100 000*g* for 30 min at 4 °C, and the supernatants (soluble protein

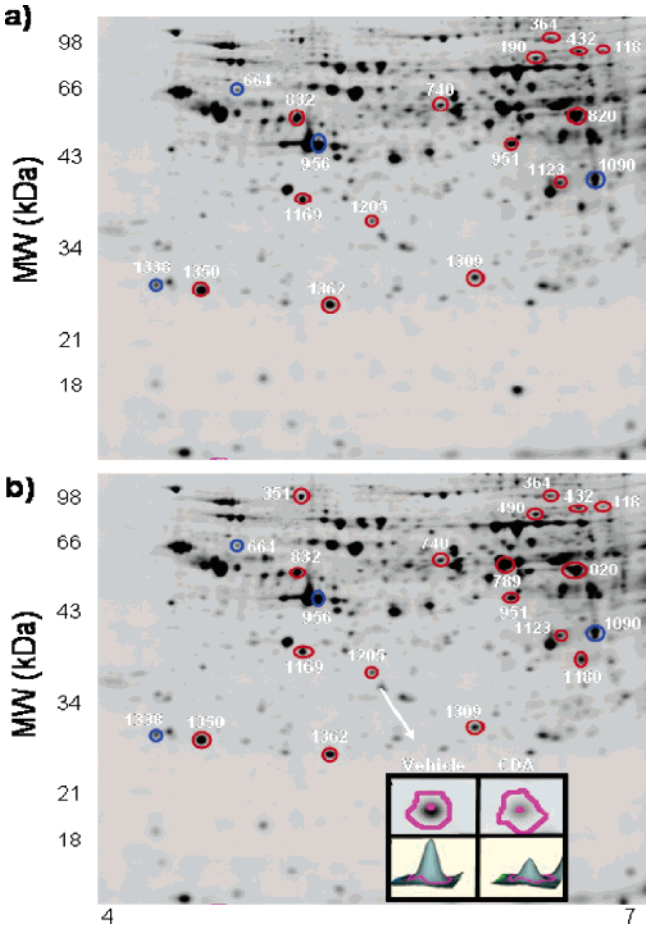

Figure 2. Protein expression changes in rat liver soluble fraction induced by treatment with CDA. 2D-DIGE images showing protein expression differences in fraction I of liver tissue following treatment of rats with CDA for (a) 2 and (b) 5 days. Blue annotations indicate protein spots which were up-regulated, and red indicates protein spots which were down-regulated in CDA-treated rats compared to vehicle-treated controls. The inset 2D and 3D images indicate spot 1205 which was used as an example for MALDI-TOF MS and Q-TOF MS/MS sequencing shown in Figure 3. The images are representative of similar results obtained from three different CDA/vehicle comparisons, each run in duplicate using the reciprocal CyDye-labeling strategy. The approximate molecular weights (MW) in kilodaltons (kDa) and isoelectric points (pI) are indicated.

Table 3. (A) Experimental and Theoretical Masses of the Peptides Recognized from the MALDI-TOF MS Analysis of Spot 1205 Identified as Rat 3-HAO, and (B) Experimental and Theoretical Masses of the Peptides Recognized from the ES Q-TOF MS/MS Analysis Belonging to Rat 3-HAO

(A)

m/z submitted	MH^+ matched	delta ppm	modifications	start	end	missed cleavages	database sequence
820.4103	820.4430	−40		89	95	0	(R) VPHSPQR (F)
919.3851	919.4274	−46		9	15	0	(K) SWVEENR (A)
967.4516	967.4961	−46		66	73	0	(R) VLEQGEHR (D)
985.4375	985.4856	−49		185	192	0	(K) AWLESHSR (E)
1043.5017	1043.5526	−49		167	175	0	(K) EPPFPLSTR (S)
1091.5219	1091.5672	−42		34	43	0	(K) IMFVGGPNTR (K)
1107.5086	1107.5621	−48	1Met-ox	34	43	0	(K)IMFVGGPNTR(K)
1126.5780	1126.6261	−43	pyroGlu	79	88	0	(R)QGEIFLLPAR(V)
1143.6098	1143.6526	−37		79	88	0	(R) QGEIFLLPAR (V)
1146.5613	1146.5907	−26		7	15	1	(R) VKSWVEENR (A)
1147.5390	1147.5570	−16		16	25	0	(R) ASFQPPVCNK (L)
1235.5628	1235.6054	−35	1Met-ox	108	117	1	(R)RMETELDGLR(Y)
1250.5972	1250.6567	−48		96	106	0	(R) FANTMGLVIER (R)
1266.5885	1266.6516	−50	1Met-ox	96	106	0	(R)FANTMGLVIER(R)
1549.7785	1549.8451	−43		66	78	1	(R) VLEQGEHRDVVIR (Q)
1577.6693	1577.7375	−43		118	130	0	(R) YYVGDTEDVLFEK (W)
2235.1211	2235.2137	−41		156	175	1	(R) TGKPNPDQLLKEPPFPLSTR (S)

(B)

observed (*m/z*)	M_r(expt) (Da)	M_r(calc) (Da)	error (Da)	peptide
476.181	950.346	950.346	0.046	SWMEENR
574.241	1146.466	1146.549	0.083	ASFQPPVCNK
554.247	1106.478	1106.554	0.076	IMFVGGPNTR
572.287	1142.558	1142.645	0.087	QGEIFLLPAR
633.785	1265.554	1265.644	0.090	FANTMGLVIER
540.217	1078.418	1078.496	0.078	METELDGLR
789.317	1576.618	1576.730	0.112	YYVGDTEDVLFEK
522.236	1042.456	1042.545	0.089	EPPFPLSTR
815.352	1630.688	1630.798	0.110	AQGSVALSVTQDPACK

fraction) were removed and stored at −80 °C. The pellets (insoluble fraction) were homogenized in 30 mM Tris (pH 8) containing 7 M urea, 2 M thiourea, and 4% CHAPS and centrifuged as above. The supernatants were removed and stored at −80 °C.

Labeling Proteins with Cyanine Dyes and Analytical 2D Gel Electrophoresis. Two different pooled standards were generated for soluble and insoluble extracts. These were made by combining equal aliquots all liver or hepatocyte extracts. Extracts and pooled standards were labeled prior to electrophoresis with the CyDyes as described previously (*8*). Briefly, pooled Cy2-labeled extracts were combined with the Cy3-labeled extracts from compound-treated rats/hepatocytes and Cy5-labeled extracts from the corresponding vehicle treatments (Table 1). A reciprocal mixture was also used to account for any preferential labeling of the CyDyes in which Cy2-labeled standard pool extracts were combined with Cy5-labeled vehicle extracts and Cy3-labeled compound extracts. These mixtures were introduced into rehydrated 18 cm IPG strips (pH 4−7) by anodic cup loading, and isoelectric focusing (IEF) was carried out at 200 V (1 h), 500 V (1 h), 1000 V (1 h), and 8000 V (8 h) at 20 °C with a maximum current setting 50 μA/strip in an IPGphor isoelectric focusing unit (Amersham Pharmacia Biotech) as described (*8*). Following IEF, the IPG strips were equilibrated for 20 min in 125 mM Tris (pH 6.8) containing 30% (v/v) glycerol, 2% (w/v) SDS, and 1% DTT, and then for a further 20 min in the same buffer except that DTT was replaced with 5% iodoacetamide. The IPG strips were then sealed with 0.5% agarose in SDS running buffer at the top of slab gels (280 mm × 210 mm × 1 mm) polymerized from 12% (w/v) acrylamide and 0.1% *N*,*N*′-methylenebisacrylamide between low fluorescent Pyrex glass plates, and second-dimension electrophoresis was carried out in Ettan Dalt II tanks (Amersham Biosciences) at 1 W/gel for 20 h.

Image Analysis. Cy2-, Cy3-, and Cy5-labeled protein images were produced by scanning gels directly between the glass plates using filters specific for each dye's excitation and emission wavelength with the Typhoon 9410 Variable Mode Imager (Amersham Biosciences) as described (*8*). Images were exported as 16-bit-tagged image file format (TIFF) files for automated analysis using the DeCyder Batch Processor and DIA software modules (Amersham Biosciences). On individual gels, Cy2-labeled images (from the pooled standard) were compared with either the Cy3 (Cy2:Cy3) or Cy5 (Cy2:Cy5) images from the individual compound and vehicle extracts using the DIA software. Images from separate gels were matched with the BVA module of the DeCyder software using the Cy2-labeled pooled standard on each gel for normalization. Results were given as standard abundance ratios for each protein spot (compound treatment relative to vehicle treatment). The statistical significance of each expression level was calculated using Student's *t*-test on the logged ratios (log compound/vehicle). Protein spot expression levels which showed statistically significant ($p < 0.05$) differences were accepted as being differentially expressed between the compound and vehicle protein extracts.

Protein Identification. Individual compound and vehicle protein extracts (300 μg) were subjected to 2D gel electrophoresis on separate preparative gels as above. Gels were post-stained with SyproRuby according to the manufacturer's instructions. After imaging, protein spots of interest were excised using the ProPic spot picking robot (Perkin-Elmer, Cambs., U.K.). Excised gel spots were digested in situ with sequencing grade porcine trypsin (*14*) using the ProGest digest robot (Perkin-Elmer). Aliquots (1 μL) of extracted digests were mixed with 0.5 μL of α-cyano-4-hydroxycinnamic acid [10 mg/mL (w/v)] dissolved in a 50:50 acetonitrile/H_2O mixture containing 0.1% trifluoroacetic acid, applied to MALDI-TOF target plates (Applied Biosystems, CA), and dried for 15 min. Peptide mass determinations were carried out using the Voyager-DE STR Biospectrometry Workstation (Applied Biosystems). Internal mass calibration was achieved using porcine trypsin autolysis digestion products. Proteins were identified by searching the Swiss-Prot and GenPept databases using MS−Fit (Protein Prospector, UCSF, CA). All searches were carried out using a mass window from 10 000 to 200 000 Da and included all rodent and human sequences. The search parameters allowed for carboxyamidomethylation of cysteine, oxidation of methionine, and modification of glutamine to pyroglutamic acid. Positive identifications were accepted with at least six matching peptide masses and at least 30% peptide coverage of the theoretical sequences. Peptides were excluded if their masses corresponded to those

for porcine trypsin and human keratins.

Networks, Pathways, and Functional Mapping. Predominant interaction networks and high-level functions of differentially expressed proteins were identified using the Ingenuity Pathways Knowledge Base (www.ingenuity.com) as described in recent reports (*15*, *16*). This analysis uses computational algorithms to identify local networks that are particularly enriched in the dataset. These local networks are preferentially enriched for the most highly connected focus proteins which have specific interactions with the other proteins in the network. The predominant functions associated with these networks were calculated using the right-tailed Fisher's Exact Test by comparing the number of proteins that participate in a given function relative to the total number of occurrences of these proteins in all functional annotations stored in the Ingenuity Pathways Knowledge Base. The Ingenuity Pathways Knowledge Base was also used to identify global functions over-represented by the entire dataset of differentially expressed proteins, and the significance values for these analyses were as calculated as above. We have also given additional weighting to functions or pathways containing the highest proportion of focus proteins relative to the number of proteins in the entire dataset of differentially expressed proteins.

Results

Histological Studies of CDA-Induced Liver Toxicity. Histological analysis of livers from rats dosed with 250 (mg/kg)/day CDA showed the occurrence of steatosis in a time-dependent manner (Figure 1). A low degree of staining was observed after 6 h of treatment, although after 2 days mild steatosis was apparent and treatment for 5 days resulted in severe steatosis. Interestingly, increased serum transaminase activity was only detected after 5 days of treatment in association with the severest manifestation of steatosis (*4*). Our previous proteomic study looking at the effects of CDA treatment identified a proteomic signature that preceded the overt toxicity seen at the longer time periods of dosing (*4*). To gain further insight into the mechanism of CDA toxicity and to identify proteomic markers associated with overt steatosis and other indications of liver toxicity such as high transaminase levels, we carried out a comparative proteomic study looking at the changes in protein abundance which occurred after 2 and 5 days treatment with CDA.

Comparative Proteomic Analysis. Liver tissues were extracted by differential solubility into soluble and insoluble fractions as outlined in Experimental Procedures following treatment of rats with either vehicle or CDA for 2 or 5 days. These were analyzed by 2D-DIGE as indicated in Table 1. Approximately 1500 protein spots were displayed on the large format 2D gels using the soluble liver extracts after both 2 and 5 days of treatment with CDA (Figure 2). Treatment with CDA for 2 days resulted in significantly altered expression of 19 protein spots. Two additional spots were altered after 5 days of treatment (Table 2). For the 5 day treatment period, 17 spots were down-regulated and 4 were up-regulated by CDA treatment (Table 2). Of the total spots, 14 (67%) produced sufficient MALDI-TOF mass fingerprints or Q-TOF MS/MS sequences according to the criteria outlined in Experimental Procedures, resulting in identification of 14 different proteins (none of these differentially expressed proteins were comprised of multiple spots). An example of one differential expressed protein (spot 1205) identified by mass fingerprinting and MS/MS sequencing, 3-hydroxyanthranilate 3,4 dioxygenase (3-HAO), is given in Table 3. The entire dataset was used for the interaction network and functional mapping analyses indicated below.

The same analysis was also carried out for the insoluble protein fraction. Approximately 2000 spots were detected for

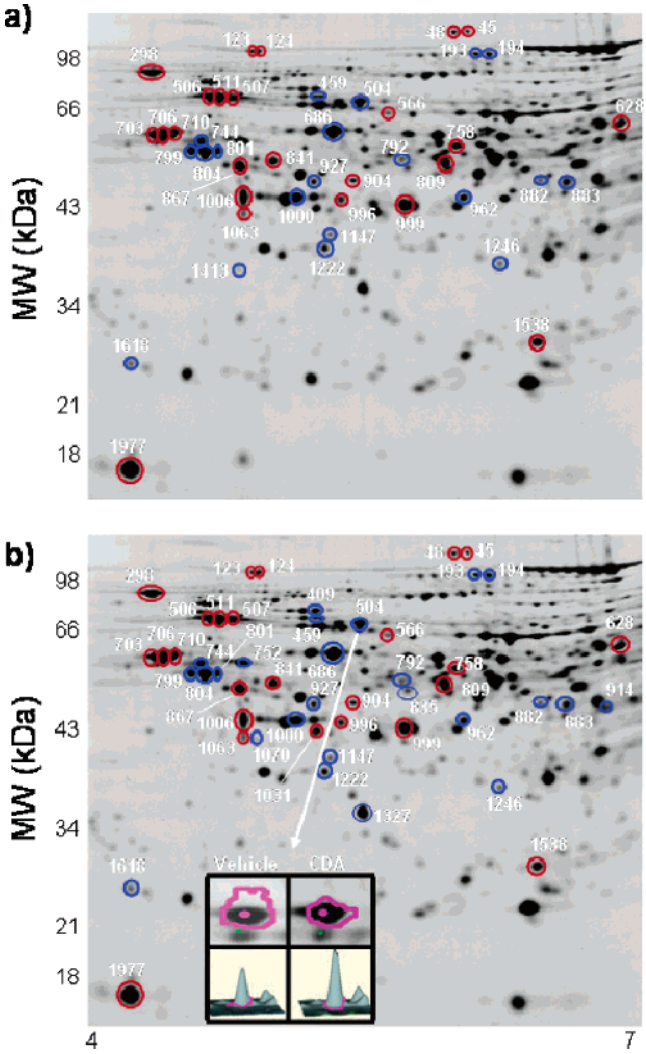

Figure 3. Protein expression changes in rat liver insoluble fraction induced by treatment with CDA. 2D-DIGE images showing protein expression differences in fraction II of liver tissue following treatment of rats with CDA for (a) 2 and (b) 5 days. Blue annotations indicate protein spots which were up-regulated, and red indicates protein spots which were down-regulated in CDA-treated rats compared to vehicle-treated controls. The images are representative of similar results obtained from three different CDA/vehicle comparisons, each comparison run in duplicate using the reciprocal CyDye-labeling strategy. The approximate molecular weights (MW) in kilodaltons (kDa) and isoelectric points (pI) are indicated.

both treatment periods (Figure 3). After the 2 day treatment period, 45 protein spots showed significant changes in abundance and 49 spots showed changes after 5 days (Table 4). For the 5 day treatment period, 25 spots were down-regulated and 24 were up-regulated. Five spots (409, 752, 914, 1031, and 1327) showed significant changes in abundance only after the 5 day treatment period, and 2 spots (432 and 1413) were changed only at the 2 day time point. Of the total differentially expressed spots in the insoluble fraction, 38 (75%) produced sufficient MALDI-TOF mass fingerprints or Q-TOF MS/MS sequences, resulting in identification of 29 different proteins (some of the differentially expressed proteins were comprised of multiple spots). An example of one differentially expressed protein (spot 504) identified by mass fingerprinting and MS/MS sequencing as GRP75/mitochondrial hsp 70 is given in Table 5. This dataset of differentially expressed proteins was combined with that obtained for the soluble fraction for use in the interaction network and functional mapping analyses indicated below.

Table 4. Identification of Insoluble Liver Proteins Which Showed Altered Expression after Treatment with CDA[a]

spot	FC 2 day	FC 5 day	ANOVA	ACC	gene name	protein
45	−1.30	−1.86	7.9×10^{-7}	ND	ND	ND
48	−1.23	−1.74	1.7×10^{-8}	ND	ND	ND
123	1.12	1.20	3.4×10^{-6}	ND	ND	ND
124	−1.19	−1.96	3.5×10^{-2}	ND	ND	ND
193	1.25	1.27	5.2×10^{-7}	ND	ND	ND
194	−1.15	−2.47	3.9×10^{-3}	ND	ND	ND
298	−1.88	−2.54	1.7×10^{-6}	P08113	TRA1	endoplasmic reticulum GRP94
409	1.01	1.37	4.4×10^{-4}	Q16891	IMMT	mitofilin
432	1.21	1.00	3.4×10^{-2}	Q6P688	MAT2A	*S*-adenosyl methionine synthase
459	1.25	1.23	1.2×10^{-3}	P48721	HSPA9	GRP75/pre-mitochondrial HSP70
504	1.31	1.51	$7.5E \times 10^{-5}$	P48721	HSPA9	GRP75/pre-mitochondrial HSP70
506	−1.39	−1.58	5.5×10^{-6}	P06761	HSPA5	endoplasmic reticulum GRP78
507	−1.47	−1.95	7.2×10^{-4}	P06761	HSPA5	endoplasmic reticulum GRP78
511	−1.96	−2.36	1.6×10^{-6}	P06761	HSPA5	endoplasmic reticulum GRP78
566	−1.24	−1.58	3.7×10^{-4}	ND	ND	ND
628	−2.20	−2.43	1.4×10^{-4}	ND	ND	ND
686	1.19	1.17	1.8×10^{-3}	P63039	HSPD1	60 kDa heat shock protein
703	−1.26	−1.39	6.2×10^{-6}	P04785	P4HB	protein disulfide isomerase (PDI)
706	−1.26	−1.35	1.3×10^{-4}	P04785	P4HB	protein disulfide isomerase (PDI)
710	−1.34	−1.41	8.9×10^{-4}	P04785	P4HB	protein disulfide isomerase (PDI)
744	1.23	1.27	1.4×10^{-3}	P09653	TBB5	tubulin β-5 chain
752	1.08	1.25	9.1×10^{-4}	P68373	TUBA6	tubulin α-6 chain
758	−1.24	−1.93	7.4×10^{-4}	Q8R086	SUOX	sulfite oxidase
792	2.08	1.97	5.3×10^{-5}	P04176	PAH	phenylalanine-4-monooxygenase
799	1.27	1.23	3.5×10^{-4}	P72247	ATPD	ATP-synthase β-chain
801	1.36	1.21	2.5×10^{-2}	P72247	ATPD	ATP-synthase β-chain
804	1.32	1.26	8.1×10^{-3}	P72247	ATPD	ATP-synthase β-chain
809	−1.45	−1.65	4.9×10^{-3}	P04176	PAH	phenylalanine-4-monooxygenase
841	−1.18	−1.83	5.2×10^{-3}	P05784	KRT18	cytokeratin 18
867	−1.54	−1.84	1.2×10^{-6}	Q63081	PDIA6	protein disulfide-isomerase A6
882	1.77	1.35	5.6×10^{-4}	ND	ND	ND
883	1.54	1.55	1.4×10^{-2}	P04182	OAT	ornithine aminotransferase
904	−1.64	−1.44	4.2×10^{-5}	ND	ND	ND
914	1.00	1.19	3.4×10^{-2}	P12007	IVD	isovaleryl-CoA dehydrogenase
927	1.21	1.40	1.9×10^{-5}	P60843	EIF4A1	eukaryotic initiation factor 4A-I
962	1.17	1.28	7.9×10^{-4}	P28330	ACADL	acyl-CoA dehydrogenase, long-chain specific
996	−1.27	−1.30	2.3×10^{-4}	ND	ND	ND
999	−1.47	−1.62	3.9×10^{-4}	ND	ND	ND
1000	1.13	1.41	1.6×10^{-3}	Q96HG5	ACTB	β actin
1006	−1.54	−1.85	3.0×10^{-3}	P55159	PON1	serum paraoxonase
1031	1.00	−1.44	1.2×10^{-3}	P19112	FBP1	fructose-1,6-biphosphatase
1063	−1.60	−2.00	4.0×10^{-3}	P55159	PON1	serum paraoxonase
1070	1.08	1.42	5.0×10^{-2}	Q9R0N0	GALK1	galactokinase
1147	1.28	1.41	3.4×10^{-2}	P21839	BCKDHB	2-oxoisovalerate dehydrogenase
1222	1.28	1.35	1.4×10^{-4}	P49432	PDHB	Pyruvate dehydrogenase (PDHE1-B)
1246	1.22	1.29	2.5×10^{-2}	ND	ND	ND
1327	1.06	1.48	2.1×10^{-3}	P67779	PHB	prohibitin
1413	1.32	1.00	7.2×10^{-3}	P02650	APOE	apolipoprotein E
1538	−2.35	−2.34	1.8×10^{-6}	Q9Z0V5	PRDX4	peroxiredoxin 4
1618	1.25	1.57	1.2×10^{-4}	P35434	ATP5D	mitochondrial H-ATP synthase, δ subunit
1977	−1.58	−1.64	3.9×10^{-5}	P00173	CYB5	cytochrome B5

[a] Protein spots indicated in Figure 3 were identified by MALDI-TOF mass fingerprinting and or Q-TOF MS/MS sequencing as described in Experimental Procedures. For each protein spot, the fold change (FC), ANOVA, protein accession number (ACC), gene names, and protein names are indicated. Only protein spots that were present on every gel and demonstrating changes of ± 0.10 with significance $p < 0.05$ were accepted as being differentially expressed. The levels of significance are given for three separate animal comparisons (each comparison carried out in duplicate incorporating reciprocal labeling). Nonidentified proteins are indicated by ND.

Interaction Networks and Functional Mapping of the Liver Proteomic Changes Following Treatment of Rats with CDA. To provide insights into the effects of CDA on liver homeostasis, functional analyses were carried out on the datasets using the Ingenuity Pathways Knowledge Base as described in Experimental Procedures. This software allows profiling data to be analyzed in a systematic way using known protein−protein interactions to determine the most significant networks, global functions, and pathways represented by the proteins undergoing change (*15*, *16*). The identified proteins were mapped onto networks available in the Ingenuity database and ranked by score. The scores take into account the number of focus proteins and the size of the network to approximate the significance of the network to the original list of focus proteins. Networks with scores of 10 or higher (negative log of the *P* value) have a high confidence of not being generated by random chance alone.

Out of 45 identified liver proteins that showed altered expression after CDA treatment, 23 were eligible for network analysis based on the Ingenuity Pathway Knowledge Base criteria. The eligibility is determined by the presence of the gene in the Ingenuity Pathway Knowledge Base. For the 2 day treatment period, the highest scoring network incorporated 9 focus proteins: apolipoprotein E (APOE), dynamin 2 (DNM2), eukaryotic initiation factor 4A1 (EIF4A1), α enolase (ENO1), 78 kDa glucose-regulated protein precursor (HSPA5), cytokeratin 18 (KRT18), cytokeratin 8 (KRT8), serum paraoxonase (PON1), and 94 kDa endoplasmic reticulum glucose-regulated protein (TRA1) (Figure 4a). The most significant function associated with this network was cell death. Consistent with this function, the network predicted interactions with cell death-associated proteins such as Tumor necrosis factor receptor type 1 associated death domain protein (TRADD), which is involved in cell death signaling (*17*). Not surprisingly, the network also predicted involvement of the transcription factor C-fos [FOS] which has been previously associated with cell death and apoptotic pathways (*17*) and has also been shown to be induced in liver by chemical hepatotoxins such as carbon tetrachloride, potentially as part of the liver recovery process (*18*). The most significant global functions and pathways associated with the entire dataset of proteins that were altered by CDA treatment for 2 days were cell death and cellular assembly and organization (Figure 4a). The identification of cellular assembly and orga-

Table 5. (A) Experimental and Theoretical Masses of the Peptides Recognized by MALDI-TOF MS Analysis of Spot 504 as Rat GRP75/Mitochondrial hsp 70, and (B) Experimental and Theoretical Masses of the Peptides Recognized from the ES Q-TOF MS/MS Analysis to Belong to Rat GRP75/Pre-Mitochondrial Heat Shock Protein 70

(A)

m/z submitted	MH^+ matched	delta ppm	modifications	start	end	missed cleavages	database sequence
887.4727	887.5137	−46	1Met-ox	100	107	1	(R)LVGMPAKR(Q)
938.4142	938.4332	−20		568	574	1	(K) YAEEDRR (K)
1045.5511	1045.5392	11	1Met-ox	647	654	1	(K)LFEMAYKK(M)
1148.5529	1148.5548	−1.6		625	634	1	(R) KDSETGENIR (Q)
1242.6933	1242.6806	10		207	218	0	(K) DAGQISGLNVLR (V)
1290.6849	1290.6806	3.3		395	405	0	(K) VQQTVQDLFGR (A)
1462.7618	1462.7576	2.9	1Met-ox	378	391	0	(K) SDIGEVILVGGMTR(M)
1476.7363	1476.7334	2.0		86	99	0	(R) TTPSVVAFTPDGER (L)
1592.9734	1592.9528	13		499	513	0	(K) LLGQFTLIGIPPAPR (G)
1608.8013	1608.7692	20	1Met-ox	174	187	1	(K)MKETAENYLGHTAK(N)
1673.8995	1673.8975	1.2		395	409	1	(K) VQQTVQDLFGRAPSK (A)
1694.8561	1694.8502	3.5		188	202	0	(K) NAVITVPAYFNDSQR (Q)
1706.8348	1706.8383	−2.0	1Met-ox	293	307	1	(R)ETGVDLTKDNMALQR(V)
1707.8492	1707.8455	2.2	pyroGlu	108	122	1	(R)QAVTNPNNTFYATKR(L)
1724.8873	1724.8720	8.9		108	122	1	(R) QAVTNPNNTFYATKR (L)
1724.8873	1724.8720	8.9		107	121	1	(K) RQAVTNPNNTFYATK (R)
2056.0035	2055.9623	20		266	284	0	(K) STNGDTFLGGEDFDQALLR (H)

(B)

observed (*m/z*)	M_r(expt) (Da)	M_r(calc) (Da)	error (Da)	peptide
738.900	1475.784	1475.726	−0.058	TTPSVVAFTPDGER
645.850	1289.684	1289.673	−0.011	VQQTVQDLFGR
574.796	1147.576	1147.547	−0.029	KDSETGENIR
616.349	1230.682	1230.657	−0.025	QAASSLQQASLK

nization as one of the predominant functions is interesting considering the findings of previous studies which showed significant changes in cytoskeletal architecture following compound-induced toxicity (*19*−*22*).

For the 5 day treatment, the highest scoring network incorporated 15 focus proteins: acyl-coenzyme A oxidase 1 (ACOX1), actin-related protein 3 (ACTR3), cytochrome B5 (CYB5), dynamin 2 (DNM2), eukaryotic initiation factor 4A1 (EIF4A1), α enolase (ENO1), glycerol dehydrogenase (GPD1), 78 kDa glucose-regulated protein precursor (HSPA5), heat shock protein 60 kDa (HSPD1), cytokeratin 18 (KRT18), cytokeratin8 (KRT8), protein disulfide-isomerase precursor (P4HB), prohibitin (PHB), and 94 kDa endoplasmic reticulum glucose-regulated protein (TRA1) (Figure 4b). As for the 2 day treatment, the most significant function associated with the 5 day treatment network was cell death. Again, FOS was implicated in this pathway, as were other proteins involved in apoptosis signaling such as the toll-like receptor 2 (TLR2) (*23*). Similar to the 2 day treatment, the most significant global functions associated with the 5 day treatment period were cell death and cellular assembly and organization (Figure 4b). However, the higher number of proteomic changes seen with the 5 day treatment period also resulted in significant alterations of two canonical signaling pathways as assessed by the Ingenuity Pathways Knowledgebase: glycolysis/gluconeogenesis and propanoate metabolism (Figure 4b). The effects on both of these pathways are not surprising given the effects of CDA on fatty acid metabolism.

Effects of CDA on Rat Hepatocytes. To determine if the CDA induced neutral lipid accumulation in hepatocytes, cells were cultured in the presence of 75−600 μM CDA. Amiodarone was used as a positive control for drug-induced neutral lipid accumulation and was tested over a concentration range of 12.5−100 μM. After 24 h of treatment, the hepatocytes were exposed to Nile Red for 4 h to measure fat accumulation. Confocal imaging showed that both compounds induced neutral lipid accumulation compared to the DMSO control treatment (Figure 5a). Hepatocytes treated with CDA at 600 μM showed more diffuse Nile Red staining compared to those treated with the lower 300 μM concentration. This is consistent with the more diffuse staining observed with neutral lipid accumulation rather than the more punctuate staining observed associated with phospholipids accumulation. Hepatocyte morphology was also more severely affected after treatment with the higher concentration of CDA as judged by the obscurity of cellular nuclei which could only be visualized at the lower concentration. This may be due to the higher levels of diffuse neutral lipid in hepatocytes treated with 600 μM CDA, which would lead to more frank cytolytic toxicity. DMSO-treated rat hepatocytes showed no fluorescence staining. Quantitation of the fluorescent Nile Red stain showed that CDA caused significant neutral lipid accumulation at 300 and 600 μM after 24 h of treatment (Figure 5b). Amiodarone also showed significant neutral lipid accumulation at 50 and 100 μM, which is consistent with the doses associated with mitochondrial oxidation inhibition.

Cultured rat hepatocytes were treated for 24 h with 600 μM CDA to determine if there was a in vitro correlation with the in vivo effects seen in rat liver. Proteins were extracted sequentially, and the insoluble fraction was analyzed by 2D-DIGE, given that this fraction yielded a higher proportion of CDA-regulated proteins in the rat liver studies (Tables 2 and 4). Approximately 900 protein spots were detected in rat hepatocytes, and 37 of these showed a significant change in abundance following treatment with CDA compared to the DMSO treatment (Figure 6a). Seventeen of these spots were down-regulated, and 20 were up-regulated. Comparison between cultured rat hepatocyte and liver proteomes showed a similarity in spot patterns, and MALDI-TOF mass fingerprinting analysis of some of the CDA-regulated spots showed that these were identical to the most abundant proteins affected by CDA in the rat liver in vivo studies (Figure 6b; Table 6). Fourteen protein spots were identified comprising 8 different proteins: β actin (ACTB),

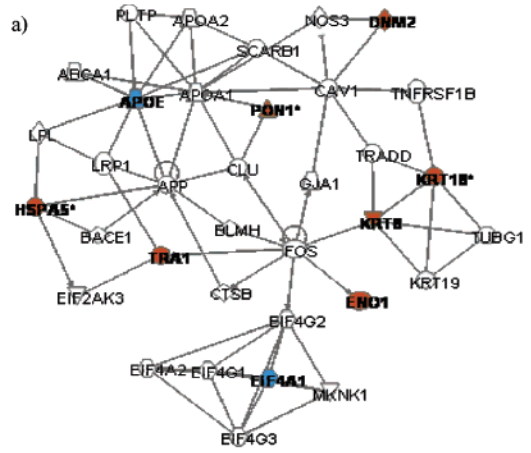

Combined soluble and insoluble proteins that showed altered expression after CDA treatment for 2 days were analyzed by Ingenuity Pathway Analysis tool as described in the experiment section.

Score	17	Network function	p-value
Focus proteins	9	Cell death	3.96E-6

Global Functions

Network	P value	Focus Proteins	Focus Protein ID
Cell death	0.00012	9	APOE CYB5, DNM2, ENO1 HSPA5*, KRT18*, KRT8, P4HB, TRA1
Cellular assembly & organization	0.000002	8	APOE, DNM2, EIF4A1, HSPA5* KRT8, KRT18*

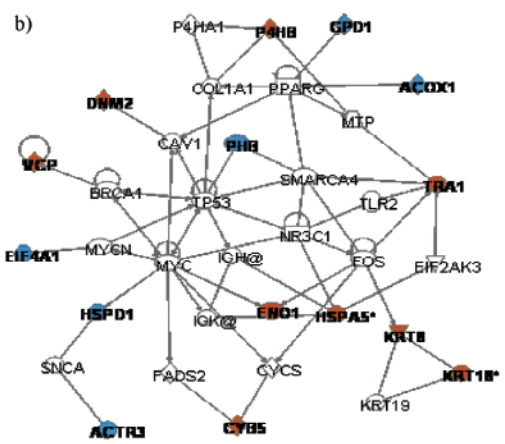

Combined soluble and insoluble proteins that showed altered expression after CDA treatment for 5 days were analyzed by Ingenuity Pathway Analysis tool as described in the experiment section.

Score	30	Network function	p-value
Focus proteins	15	Cell death	6.01E-6

Global Functions

Network	P value	Focus Proteins	Focus Protein ID
Cell death	0.000001	12	ALDH* CYB5, DNM2, ENO1, HSP60, HSPA5*, KRT18*, KRT8, P4HB, PHB, TRA1, VCP
Cellular assembly & organization	0.000002	8	ACOX1, ACTR3 DNM2, EIF4A1 HSPA5* KRT8, KRT18*, VCP

Global Canonical Pathways

Network	P value	Focus Proteins	Focus Protein ID
Glycolysis & Gluconeogenesis	0.0034	4	ALDH* CYB5, DNM2, ENO1, HSP60, HSPA5*, KRT18*, KRT8, P4HB, PHB, TRA1, VCP
Propanoate metabolism	0.0089	4	ACOX1, ACTR3 DNM2, EIF4A1 HSPA5* KRT8, KRT18*, VCP

Figure 4. Networks of liver proteins regulated by CDA treatment. Combined soluble and insoluble proteins that showed altered expression after CDA treatment were analyzed by the Ingenuity Pathway Analysis tool as described in Experimental Procedures. Twenty-three nonredundant proteins (out of 45 input proteins) were eligible for network analysis, and the networks were scored according to significance and number of focus proteins (bold type) within the network. Only networks with a score greater than 10 are indicated. The top functions associated with each network are also indicated. Thirty proteins were eligible for global function/pathways analysis which were ranked according to significance and the number of associated (focus) proteins. The focus proteins are indicated by their gene names. Blue and red symbols/text represent up- and down-regulated proteins, respectively. Asterisks indicate proteins that appeared as multiple spots.

aldehyde dehydrogenase (ALDH2), ATP-synthase β-chain (ATPD), dynamin 2 (DNM2), 78 kDa glucose-regulated protein precursor (HSPA5), heat shock protein 60 kDa (HSPD1), tubulin β-5 chain (TBB5), and protein disulfide isomerase (P4HB). All of the protein spots comprising these proteins showed the same directional change as seen in the in vivo study with the exception of β actin which was both up-regulated (spot 630) and down-regulated (spots 607 and 627) in the hepatocytes (Table 6) compared to only one up-regulated spot (spot 1000) seen in the rat liver proteome (Table 4). One other difference was that, in the hepatocytes, the heat shock protein 60 kDa was comprised of a string of 5 spots which were all up-regulated by CDA treatment, whereas only one up-regulated spot was detected for the same protein in the rat liver proteome (Figure 6b). Nevertheless, this suggested that the core protein was regulated similarly by CDA in both the rat hepatocytes and liver samples.

Given the significant affects on neutral lipid accumulation following CDA treatment, rat hepatocytes were also assessed for any effects of CDA or amiodarone on mitochondrial dehydrogenase activity using the MTT substrate. Hepatocytes showed a significant decrease in MTT cleavage after 24 h of treatment with both 300 and 600 μM CDA, although the effect was markedly changed at the higher concentration (Figure 7). Amiodarone, which is known to inhibit mitochondrial activity, also showed a significant decrease in mitochondrial activity at concentrations of 25 μM and above (Figure 7).

Discussion

Late stage failures of drug candidates are costly to the pharmaceutical industry. One approach that pharmaceutical companies could use to address this issue is to carry out safety and efficacy studies simultaneously (*24*). This requires that toxicological studies are integrated into the discovery phase to improve the quality of drug candidates and reduce the overall cost of drug development. The application of expression profiling technologies such as transcriptomics and proteomics to mechanistic and predictive toxicology, and to biomarker discovery, could help to reduce the compound failure rate during safety studies. However, prior to achieving this goal, sound

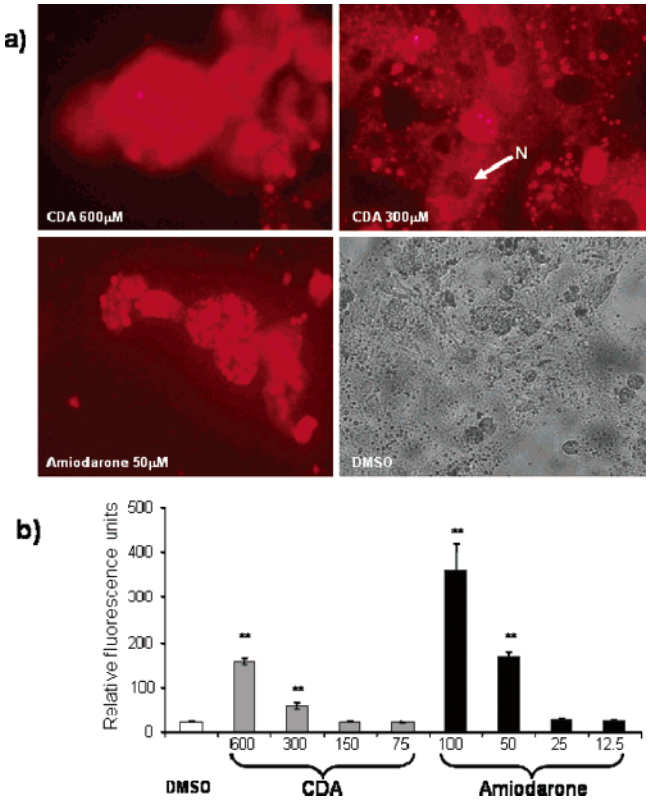

Figure 5. Effect of CDA and amiodarone on neutral lipid accumulation in rat hepatocytes. (a) Hepatocytes were incubated with 600 and 300 μM CDA, 50 μM amiodarone, or DMSO for 24 h and analyzed by confocal microscopy for Nile Red binding as described in Experimental Procedures. N = nucleus of a hepatocyte. (b) Hepatocytes were incubated for 24 h with the indicated concentrations (μM) of CDA and amiodarone and then assessed for Nile Red binding as described in Experimental Procedures. The data shown are means ± SEM (n = 6) of relative fluorescence units. DMSO was the negative control. **p < 0.01.

interpretation of information is required in these new areas of global data generation to ensure that toxicologically relevant changes are distinguished from those that are not. The other aim of these new technologies is to identify markers that could be used for following the safety and efficacy profiles of drugs within a clinical environment.

In this study, we have attempted to identify proteomic markers of drug toxicity that could ultimately be applied to facilitate the drug discovery process in a high-throughput format. This required a correlation between the in vivo and in vitro proteomic responses to treatment with a development compound designated CDA. The results obtained from the in vivo rat liver proteomic study suggested that the observed accumulation of fatty acids over the 5 day treatment period was due to perturbation of the fatty acid β-oxidation and possibly oxidative phosphorylation pathways as shown by alterations in proteins such as pyruvate dehydrogenase (P4HB), phenylalanine-4-monooxygenase (PAH), and 2-oxoisovalerate dehydrogenase (IVD) which are involved indirectly in acetyl-CoA production (*25*−*27*). The glycolytic enzyme glycerol-3-phosphate dehydrogenase (GPD1) was also up-regulated by CDA in this study, suggesting a possible intensification of glycolysis and synthesis of triacylglycerides in hepatic steatosis as reported previously in the regenerating liver model of fat accumulation (*28*, *29*). Another enzyme that was down-regulated by CDA treatment was 3-hydroxyanthranilate 3,4 dioxygenase (HAAO), which plays a role in tryptophan catabolism. Previous studies have shown that HAAO is also down-regulated in livers of hypercholesterolemic rabbits (*30*) and in that of the hyperlipidemic HcB19 mouse model (*31*).

This study also showed CDA-induced alterations in expression of proteins with a more direct role in fatty acid metabolism such as the long-chain specific acyl-CoA dehydrogenase (ACADL), which catalyzes the initial step in mitochondrial fatty acid oxidation (*32*). The current finding that ACADL was up-regulated in association with the fatty livers induced by CDA treatment is consistent with previous studies which showed an increase in this same protein in nonalcoholic fatty liver disease(*33*). Indeed, the accumulation of intracellular lipids, such as fatty acids, may lead to the activation of PPARα and the increased expression and translation of ACADL. Another protein that was up-regulated by CDA treatment with a direct role in fatty acid metabolism was propionyl-CoA carboxylase (PCCA), which is the key enzyme in the catabolic pathway of odd-chain fatty acids, isoleucine, threonine, methionine, and valine (*34*). The up-regulation of PCCA in the CDA model of steatosis is consistent with previous findings that PCCA knock-out mice showed fatty liver and fatal ketoacidosis (*35*). Also, a recent proteomic study showed that PCCA was down-regulated in the hyperlipidemic HcB19 mouse model characterized with fatty liver (*31*).

The secreted proteins serum paraoxonase (PON1) and peroxiredoxin IV (PRx IV) were down-regulated after treatment with CDA. Previous studies demostrated that PON1 was significantly decreased in rats treated with carbon tetrachloride (*36*), which has been shown to cause liver steatosis (*37*). This suggests that the CDA-induced liver steatosis might be associated with disruption of the secretory pathway and is consistent with the observed down-regulation of the endoplasmic reticulum chaperone proteins glucose-responsive protein 94 (TRA1), glucose responsive protein 78 (HSPA9), and protein disulfide isomerase (P4HB). Interestingly, dynamin, a large GTPase protein which is considered to play the pivotal role in the regulation of docking and fusion of secretory vesicles (*38*), was also down-regulated by CDA treatment. PON1 and PRxIV have been shown to play a role in detoxifying reactive species produced during oxidative stress (*39*). Therefore, the CDA-induced down-regulation of these proteins might lead to an impairment of oxidative stress protection rendering liver cells more susceptible to damage and contributing to the progression of the toxicity. This possibility was supported by the finding that aldehyde dehydrogenase (ALDH2) was also down-regulated after treatment with CDA as stated above.

Several other proteins showed significant alterations following CDA treatment, including catechol-*O*-methyltransferase (COMT), sulfite oxidase (SUOX), and ornithine aminotransferase (OAT), which have no direct links with lipid metabolism and have not been associated previously with hepatic steatosis. Further studies are required to verify the toxicological pathways activated by these proteins in response to CDA treatment.

Changes in cellular structure proteins were also observed in livers from rats treated with CDA for 2 and 5 days. Cytokeratin 8 (KRT8) was down-regulated at both time points investigated. The cytokeratins are essential for the maintenance of the hepatocyte structural and functional integrity (*40*). Recent reports have shown that imbalanced expression of cytokeratin 8 and 18 may be an important determinant in Mallory bodies formation, which occurs during the latest stages of steatosis (*41*). More recently, a link has also been reported between changes in cytokeratins 8 and 18 in liver disease progression such as cirrhosis (*42*). The expression of cytokeratin 18 (KRT18) was decreased significantly only after 5 days of treatment with CDA.

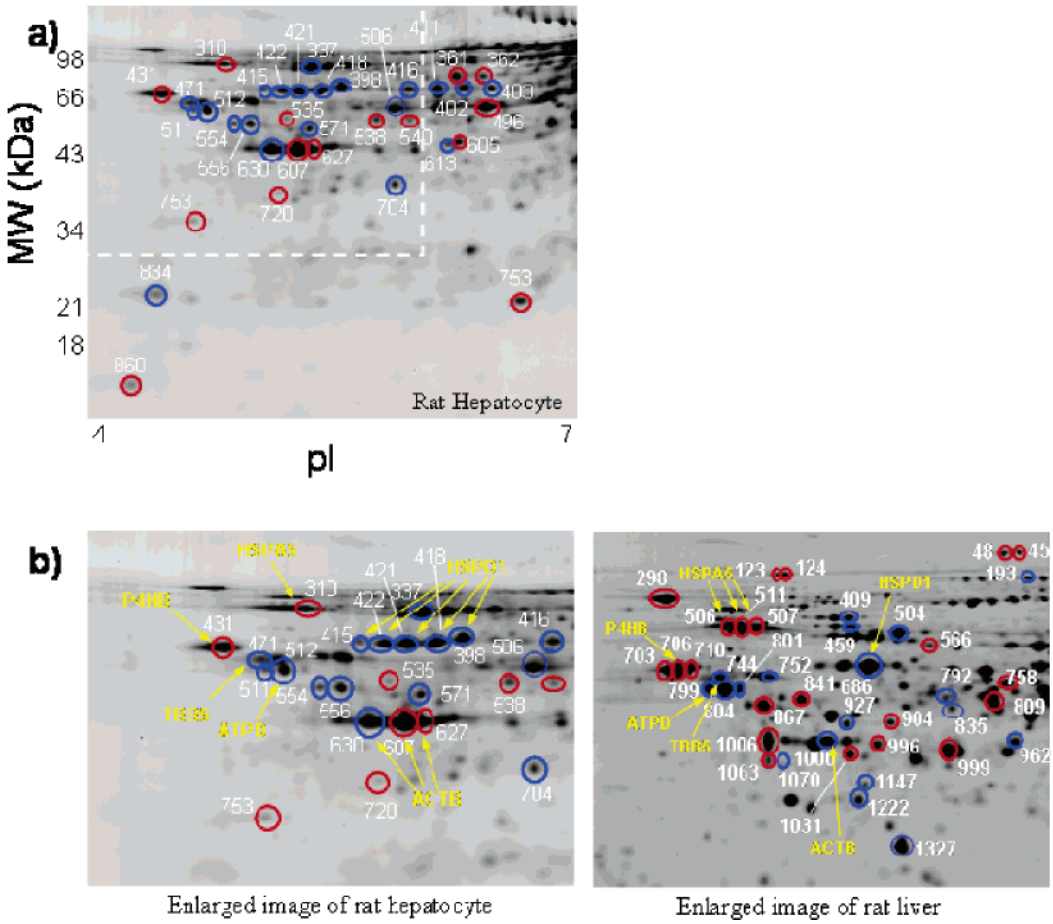

Figure 6. Correlation of CDA-induced protein expression changes in rat hepatocytes and rat liver. (a) Fluorescent image showing protein expression differences in the insoluble protein extract of rat hepatocytes following treatment with 600 μM CDA for 24 h. (b**)** Enlarged fluorescent image corresponding to the insoluble protein extract of rat hepatocytes and liver tissue (5 days treatment CDA; from Figure 4), revealing similar proteomic changes in both samples (yellow). Blue annotations indicate proteins which were up-regulated, and red annotations indicate proteins which were down-regulated following CDA treatment compared to the DMSO control treatment. The images are representative of similar results obtained from three different CDA/control comparisons. The spot numbers are taken from the corresponding master gel image. The approximate molecular weights (MW) in kilodaltons (kDa) and isoelectric points (pI) are indicated.

This is consistent with the more severe stage of steatosis observed after the 5 day treatment period with CDA, suggesting that the cell architecture is more profoundly affected after longer periods of treatment.

Treatment with CDA induced modulation of two major functions in the liver, as determined by the Ingenuity Pathways Knowledge base analysis: cell death and cellular assembly and organization. Consistent with the more severe stage of steatosis observed after 5 days of CDA treatment, the effects on cell death were more significant and comprised of more experimentally determined focus proteins after the longer treatment period.Some of the key proteins comprising this function were aldehyde dehydrogenase (ALDH2), cytochrome B5 (CYB5), dynamin(DNM2), α enolase (ENO1), heat shock protein 60kDa (HSPD1), glucose responsive protein 78 kDa (HSPA5), cytokeratin 18 (KRT18), cytokeratin 8 (KRT8), protein disulfide isomerase (P4HB), prohibitin (PHB), glucose responsive protein 94 kDa (TRA1), and transitional endoplasmic reticulum ATPase (VCP). The only significant effects on canonical signaling pathways were detected after the 5 day treatment period. These were glycolysis/gluconeogenesis and propanoate metabolism. The network analysis also highlighted several other potential markers of CDA toxicity such as tumor necrosis factor receptor type 1-associated death domain protein (TRADD), C-fos (FOS), and the toll-like receptor 2 (TLR2). Further studies will be required to confirm whether these proteins are also regulated by CDA treatment.

One interesting finding from our previous study (*4*) was that steatosis was present as early as 6 h after treatment with CDA without significant elevation of serum transaminases. Since measurement of transaminases is in widespread use as an indicator of hepatic effects from early preclinical testing to postmarket monitoring of patients (*43*), this raises the question of whether transaminase measurement can detect toxicities at the early stages. A recent report on troglitazone-induced toxicityshowed that values of hepatic enzymes were altered at some point during therapy, but 13 out of 17 patients showed normal values before liver failure (*44*). This is significant because, even when transaminases values were found to be elevated and treatment discontinued, liver failure still resulted in this study (*44*). Such evidence emphasizes the importance of considerable further work to identify earlier markers of liver toxicity in serum before a phase of irreversible damage is reached.

A desired outcome of the application of proteomics in drug discovery would be to identify markers that could be measured in a high-throughput approach that is amenable to the drug discovery process. This would require the optimization of in vitro technologies that could be applied to investigate potential toxicity liabilities of new compounds. Such an approach requires

Table 6. Identification of Insoluble Hepatocyte Proteins Which Showed Altered Expression after Treatment with CDA[a]

Spot	FC 2 day	FC 5 day	ANOVA	ACC	Gene name
310	−1.29	3.8E−005	P06761	HSPA5	Endoplasmic reticulum GRP78
337	1.34	2.1E−004			
361	−1.30	3.4E−004			
362	−1.32	3.1E−005			
398	1.28	2.2E−004	P63039	HSPD1	60 kDa heat shock protein
402	1.77	1.1E−006			
403	1.31	8.0E−005			
411	1.55	3.3E−006			
415	1.84	1.0E−006	P63039	HSPD1	60 kDa heat shock protein
418	1.40	3.2E−005	P63039	HSPD1	60 kDa heat shock protein
421	1.57	1.1E−005	P63039	HSPD1	60 kDa heat shock protein
422	1.70	1.3E−005	P63039	HSPD1	60 kDa heat shock protein
431	−1.38	1.5E−004	P04785	P4HB	Protein disulfide isomerase (PDI)
454	−3.07	9.5E−007			
471	1.27	2.7E−003	P09653	TBB5	Tubulin β−5 chain
496	−1.24	1.7E−006	P11884	ALDH2	Aldehyde dehydrogenase
506	1.16	4.8E−005			
511	1.87	1.0E−007			
512	1.66	3.8E−007	P72247	ATPD	ATP-synthase β-chain
535	−6.49	9.7E−010			
538	−2.44	4.0E−007			
540	−1.69	1.4E−006			
554	1.99	3.3E−011	P39052	DNM1	Dynamin 1
556	1.37	2.9E−008			
571	1.41	1.7E−005			
605	−1.18	4.8E−003			
607	−1.35	2.6E−007	Q96HG5	ACTB	Beta actin
613	1.42	1.3E−007			
627	−1.22	1.8E−005	Q96HG5	ACTB	Beta actin
630	1.29	4.8E−007	Q96HG5	ACTB	Beta actin
704	3.61	1.4E−007			
720	−5.44	1.3E−009			
747	−3.35	2.8E−008			
753	−4.74	1.1E−009			
834	1.39	7.0E−005			
841	−2.44	2.2E−008			
860	−1.42	4.2E−004			

[a] Protein spots indicated in Figure 6a were identified by MALDI-TOF mass fingerprinting and/or Q-TOF MS/MS sequencing as described in Experimental Procedures. For each protein spot, the fold change (FC), ANOVA, protein accession number (ACC), and gene names are indicated. Only protein spots that were present on every gel and demonstrating changes of ± 0.10 with significant.

a correlation of protein markers between in vivo studies and the appropriate in vitro model. In this study, we showed a good correlation of the proteomic markers which were altered by CDA treatment in rat liver with those observed to change in cultured rat hepatocytes. The limited mass spectrometry analysis that was carried out for these samples showed that some of the markers corresponded to the endoplasmic reticulum and mitochondrial chaperones HSPD1, HSPA5, and P4HB with similar effects also seen for ATP-synthase β-chain (ATPD), tubulin β-5 chain (TBB5), and β actin (ACTB).

The accumulation of neutral lipids in rat hepatocytes treated with CDA was confirmed using the Nile Red dye-binding assay,as previously described by McMillian and co-workers (*11*). It will be intriguing to carry out more detailed time-course studies using this in vitro toxicity model to determine whether any proteomic markers can be detected before the onset of visible neutral lipid accumulation. If this is the case, such proteomic markers would provide a more rapid readout compared to the neutral lipid accumulation studies. In addition, to use the biomarkers in regulatory submissions of new drugs, further optimization, validation, and standardization between laboratories and organizations would be required.

Previous studies have shown that steatosis is linked to impaired mitochondrial function as a result of low energy production (*6*). Such impairment has been suggested to occur through drug-induced perturbations of either the β-oxidation or oxidative phosphorylation pathways (*5*, *45*−*47*). This is consistent with the results of the in vitro study reported here, which suggested that a mitochondrial energy metabolism function was impaired. From these studies, it is not possible to establish whether CDA disrupts the β-oxidation pathway or ATP synthesis first. However, cultured rat hepatocytes treated with CDA at 300 μM for 24 h showed significant neutral lipid accumulation before a significant decrease in mitochondrial dehydrogenase activity was observed. Also, other studies have shown that excessive fatty acids, acyl-CoAs, and dicarboxylic acids have deleterious effects upon mitochondria (*6*). Taken together, these findings suggest that CDA disrupted the β-oxidation pathway first, which led to toxicity. Further mechanistic studies incorporating earlier time points and metabolic measurements would be required in order to resolve this issue.

In summary, the results generated in this study demonstrated the capacity of proteomics technologies to identify protein markers of a drug-induced toxicity even before the onset of clinical parameters changes. This study also showed the potential of using an in vitro assay to identify protein markers of the same drug-induced toxicity. However, further work would be

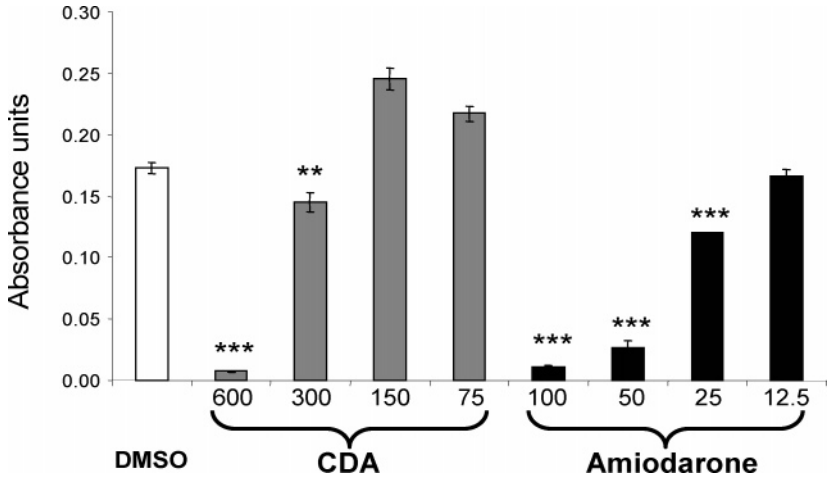

Figure 7. Effect of CDA and amiodarone on mitochondrial dehydrogenase activity. Effect of the indicated concentrations (μM) of CDA and amiodarone on MTT metabolism in cultured rat hepatocytes. Data shown are means ± SEM ($n = 6$) of relative absorbance units. DMSO was the negative control. $^{**}p < 0.01$; $^{***}p < 0.001$.

required to establish whether the proteins identified in this study could be used as a predictive signature for liver steatosis. These studies would include testing drugs known to cause liver steatosis over a range of different doses and times and performing comparative proteomics to determine common protein markers. Additionally, follow-up studies could also be designed to investigate other proteins involved in the pathways shown to be of significance by the Ingenuity Pathways Knowledge Base software.

References

(1) Cockerell, G. L., McKim, J. M., and Vonderfecht, S. L. (2002) Strategic importance of research support through pathology. *Toxicol. Pathol. 30* (1), 4−7.

(2) Wilkins, M. R., Williams, K. L., Appel, R. D., and Hochstrasser, D. F. (1997) *Proteome Research*: *New Frontiers in Functional Genomics*, Springer-Verlag, New York.

(3) Mortishire-Smith, R. J, Skiles, G. L., Lawrence, J. W., Spence, S., Nicholls, A. W., Johnson, B., and Nicholson, J. K. (2003) Use of metabonomics to identify impaired fatty acid metabolism as the mechanism of a drug-induced toxicity.

(4) Meneses-Lorente, G., Guest, P. C., Lawrence, J., Muniappa, N., Knowles, M. R., Skynner, H. A., Salim, K., Cristea, I., Mortishire-Smith, R., Gaskell, S. J., and Watt, A. (2004) A proteomic investigation of drug-induced steatosis in rat liver. *Chem. Res. Toxicol. 17* (5), 605−612.

(5) Berson, A., De Beco, V., Letteron, P., Robin, M. A., Moreau, C., El Kahwaji, J., Verthier, N., Feldmann, G., Fromentry, B., and Pessayre, D. (1998) Steatohepatitis-inducing drugs cause mitochondrial dysfunction and lipid peroxidation in rat hepatocytes. *Gastroenterology 114* (4), 764−774.

(6) Fromenty, B., and Pessayre, D. (1995) Inhibition of mitochondrial beta-oxidation as a mechanism of hepatotoxicity. *Pharmacol. Ther. 67* (1), 101−154.

(7) Unlu, M., Morgan, M. E., and Minden, J. S. (1997) Difference gel electrophoresis. A single gel method for detecting changes in protein extracts. *Electrophoresis 18* (11), 2071−2077.

(8) Knowles, M. R., Cervino, S., Skynner, H. A., Hunt, S. P., de Felipe, C., Salim, K., Meneses-Lorente, G., McAllister, G., and Guest, P. C. (2003) Multiplex proteomic analysis by two-dimensional differential in-gel electrophoresis. *Proteomics 3* (7), 1162−1171.

(9) Strom, S. C., Jirtle, R. L., Jones, R. S., Novicki, D. L., Rosenberg, M. R., Novotny, A., Irons, G., McLain, J. R., and Michalopoulos, G. (1982) Isolation, culture, and transplantation of human hepatocytes. *J. Natl. Cancer Inst. 68* (5), 771−778.

(10) Greenspan, P., Mayer, E. P., and Fowler, S. D. (1985) Nile red: a selective fluorescent stain for intracellular lipid droplets. *J. Cell Biol. 100* (3), 965−973.

(11) McMillian, M. K., Grant, E. R., Zhong, Z., Parker, J. B., Li, L., Zivin, R. A., Burczynski, M. E., and Johnson, M. D. (2001) Nile Red binding to HepG2 cells: an improved assay for in vitro studies of hepatosteatosis. *In Vitro Mol. Toxicol. 14* (3), 177−190.

(12) Kasugai, S., Hasegawa, N., and Ogura, H. (1990) A simple in vito cytotoxicity test using the MTT (3-(4,5)-dimethylthiazol-2-yl)-2,5-diphenyl tetrazolium bromide) colorimetric assay: analysis of eugenol toxicity on dental pulp cells (RPC-C2A). *Jpn. J. Pharmacol. 52* (1), 95−100.

(13) Molloy, M. P., Herbert, B. R., Walsh, B. J., Tyler, M., I, Traini, M., Sanchez, J. C., Hochstrasser, D. F., Williams, K. L., and Gooley, A. A. (1998) Extraction of membrane proteins by differential solubilization for separation using two-dimensional gel electrophoresis. *Electrophoresis 19* (5), 837−844.

(14) Wilm, M., and Mann, M. (1996) Analytical properties of the nanoelectrospray ion source. *Anal. Chem. 68* (1), 1−8.

(15) Raponi, M., Belly, R. T., Karp, J. E., Lancet, J. E., Atkins, D., and Wang, Y. (2004) Microarray analysis reveals genetic pathways modulated by tipifarnib in acute myeloid leukemia. *BMC Cancer 4*, 56.

(16) Siripurapu, V., Meth, J., Kobayashi, N., and Hamaguchi, M. (2005) DBC2 significantly influences cell-cycle, apoptosis, cytoskeleton and membrane-trafficking pathways. *J. Mol. Biol. 346* (1), 83−89.

(17) Hsu, H., Xiong, J., and Goeddel, D. V. (1995) The TNF receptor 1-associated protein TRADD signals cell death and NF-kappa B activation. *Cell 81* (4), 495−504.

(18) Bruccoleri, A., Gallucci, R., Germolec, D. R., Blackshear, P., Simeonova, P., Thurman, R. G., and Luster, M. I. (1997) Induction of early-immediate genes by tumor necrosis factor alpha contribute to liver repair following chemical-induced hepatotoxicity. *Hepatology 25* (1), 133−141.

(19) Runnegar, M. T., Andrews, J., Gerdes, R. G., and Falconer, I. R. (1987) Injury to hepatocytes induced by a peptide toxin from the cyanobacterium *Microcystis aeruginosa*. *Toxicon 25* (11), 1235−1239.

(20) Falconer, I. R., and Yeung, D. S. (1992) Cytoskeletal changes in hepatocytes induced by *Microcystis* toxins and their relation to hyperphosphorylation of cell proteins. *Chem.—Biol. Interact. 81* (1−2), 181−196.

(21) Wickstrom, M. L., Khan, S. A., Haschek, W. M., Wyman, J. F., Eriksson, J. E., Schaeffer, D. J., and Beasley, V. R. (1995) Alterations in microtubules, intermediate filaments, and microfilaments induced by microcystin-LR in cultured cells. *Toxicol. Pathol. 23* (3), 326−337.

(22) Grossmann, E. M., Longo, W. E., Kaminski, D. L., Smith, G. S., Murphy, C. E., Durham, R. L., Shapiro, M. J., Norman, J. G., and Mazuski, J. E. (2000) Clostridium difficile toxin: cytoskeletal changes and lactate dehydrogenase release in hepatocytes. *J. Surg. Res. 88* (2), 165−172.

(23) Aliprantis, A. O., Yang, R. B., Weiss, D. S., Godowski, P., and Zychlinsky, A. (2000) The apoptotic signaling pathway activated by Toll-like receptor-2. *EMBO J. 19* (13), 3325−3336.

(24) Ulrich, R., and Friend, S. H. (2002) Toxicogenomics and drug discovery: will new technologies help us produce better drugs? *Nat. Rev. Drug Discovery 1* (1), 84−88.

(25) Massey, L. K., Sokatch, J. R., and Conrad, R. S. (1976) Branched-chain amino acid catabolism in bacteria. *Bacteriol. Rev. 40* (1), 42−54.

(26) Reed, L. J., Fernandez-Moran, H., Koike, M., and Willms, C. R. (1964) Electron microscopic and biochemical studies of pyruvate dehydrogenase complex of *Escherichia coli*. *Science 145*, 930−932.

(27) Robson, K. J. H., Chandra, T., MacGillivray, R. T. A., and Woo, S. L. C. (1982) Polysome immunoprecipitation of phenylalanine hydroxylase mRNA from rat liver and cloning of its cDNA. *Proc. Natl. Acad. Sci. U.S.A. 79* (15), 4701−4705.

(28) Dzhivanian, K. A., and Ter Oganian, K. S. (1979) [Nonspecific esterase and alpha-glycerolphosphate dehydrogenase activity and the fat content in the regenerating chicken liver]. *Biull. Eksp. Biol. Med. 87* (6), 547−550.

(29) Stein, T. A., Burns, G. P., Tropp, B. E., and Wise, L. (1985) Hepatic fat accumulation during liver regeneration. *J. Surg. Res. 39* (4), 338−343.

(30) Ragazzi, E., Costa, C. V., Caparrotta, L., Biasiolo, M., Bertazzo, A., and Allegri, G. (2002) Enzyme activities along the tryptophan-nicotinic acid pathway in alloxan diabetic rabbits. *Biochim. Biophys. Acta 1571* (1), 9−17.

(31) Van Greevenbroek, M. M., Vermeulen, V. M., and De Bruin, T. W. (2004) Identification of novel molecular candidates for fatty liver in the hyperlipidemic mouse model, HcB19. *J. Lipid Res. 45* (6), 1148−1154.

(32) Skrede, S., Sorensen, H. N., Larsen, L. N., Steineger, H. H., Hovik, K., Spydevold, O. S., Horn, R., and Bremer, J. (1997) Thia fatty acids, metabolism and metabolic effects. *Biochim. Biophys. Acta 1344* (2), 115−131.

(33) Nakamuta, M., Kohjima, M., Morizono, S., Kotoh, K., Yoshimoto, T., Miyagi, I., and Enjoji, M. (2005) Evaluation of fatty acid metabolism-related gene expression in nonalcoholic fatty liver disease. *Int. J. Mol. Med. 16* (4), 631−635.

(34) Kraus, J. P., Kalousek, F., and Rosenberg, L. E. (1983) Biosynthesis and mitochondrial processing of the beta subunit of propionyl coenzyme A carboxylase from rat liver. *J. Biol. Chem. 258* (12), 7245−7248.

(35) Miyazaki, T., Ohura, T., Kobayashi, M., Shigematsu, Y., Yamaguchi, S., Suzuki, Y., Hata, I., Aoki, Y., Yang, X., Minjares, C., Haruta, I., Uto, H., Ito, Y., and Muller, U. (2001) Fatal propionic acidemia in mice lacking propionyl-CoA carboxylase and its rescue by postnatal, liver-specific supplementation via a transgene. *J. Biol. Chem. 276* (38), 35995−35999.

(36) Ferre, N., Camps, J., Cabre, M., Paul, A., and Joven, J. (2001) Hepatic paraoxonase activity alterations and free radical production in rats with experimental cirrhosis. *Metab., Clin. Exp. 50* (9), 997−1000.

(37) Weber, L. W., Boll, M., and Stampfl, A. (2003) Hepatotoxicity and mechanism of action of haloalkanes: carbon tetrachloride as a toxicological model. *Crit. Rev. Toxicol. 33* (2), 105−136.

(38) Jones, S. M., Howell, K. E., Henley, J. R., Cao, H., and McNiven, M. A. (1998) Role of dynamin in the formation of transport vesicles from the trans-Golgi network. *Science 279* (5350), 573−577.

(39) Shih, D. M., Gu, L., Xia, Y. R., Navab, M., Li, W. F., Hama, S., Castellani, L. W., Furlong, C. E., Costa, L. G., Fogelman, A. M., and Lusis, A. J. (1998) Mice lacking serum paraoxonase are susceptible to organophosphate toxicity and atherosclerosis. *Nature 394* (6690), 284−287.

(40) Loranger, A., Duclos, S., Grenier, A., Price, J., Wilson-Heiner, M., Baribault, H., and Marceau, N. (1997) Simple epithelium keratins are required for maintenance of hepatocyte integrity. *Am. J. Pathol. 151* (6), 1673−1683.

(41) Nakamichi, I., Hatakeyama, S., and Nakayama, K. I. (2002) Formation of Mallory body-like inclusions and cell death induced by deregulated expression of keratin 18. *Mol. Biol. Cell 13* (10), 3441−3451.

(42) Toivola, D. M., Ku, N. O., Resurreccion, E. Z., Nelson, D. R., Wright, T. L., and Omary, M. B. (2004) Keratin 8 and 18 hyperphosphorylation is a marker of progression of human liver disease. *Hepatology 40* (2), 459−466.

(43) Amacher, D. E. (1998) Serum transaminase elevations as indicators of hepatic injury following the administration of drugs. *Regul. Toxicol. Pharmacol. 27* (2), 119−130.

(44) Graham, D. J., Green, L., Senior, J. R., and Nourjah, P. (2003) Troglitazone-induced liver failure: a case study. *Am. J. Med. 114* (4), 299−306.

(45) Pessayre, D., Bichara, M., Degott, C., Potet, F., Benhamou, J. P., and Feldmann, G. (1979) Perhexiline maleate-induced cirrhosis. *Gastroenterology 76* (1), 170−177.

(46) Simon, J. B., Manley, P. N., Brien, J. F., and Armstrong, P. W. (1984) Amiodarone hepatotoxicity simulating alcoholic liver disease. *N. Engl. J. Med. 311* (3), 167−172.

(47) Zimmerman, H. J. (1978) *Hepatotoxicity*: *The Adverse Effects of Drugs and Other Chemicals on the Liver*, Appleton-Century-Crofts, New York.

TX060007F